Organic & Biomolecular Chemistry

ROYAL SOCIETY OF CHEMISTRY

PAPER

View Article Online
View Journal | View Issue

Cite this: *Org. Biomol. Chem.*, 2020, **18**, 8109

Total synthesis of the actinoallolides and a designed photoaffinity probe for target identification†

Matthew J. Anketell, Theodore M. Sharrock and Ian Paterson *

Received 4th September 2020,
Accepted 25th September 2020

DOI: 10.1039/d0ob01831g

rsc.li/obc

The actinoallolides are a family of polyketide natural products isolated from the bacterium *Actinoallomurus fulvus*. They show potent biological activity against trypanosomes, the causative agents of the neglected tropical diseases human African trypanosomiasis (sleeping sickness) and Chagas disease, while exhibiting no cytotoxicity against human cell lines. Herein, we give a full account of our strategy evolution towards the synthesis of this structurally unique class of 12-membered macrolides, which culminated in the first total synthesis of (+)-actinoallolide A in 20 steps and 8% overall yield. Subsequent late-stage diversification then provided ready access to the congeneric (+)-actinoallolides B–E. Enabled by this flexible and efficient endgame sequence, we also describe the design and synthesis of a photoaffinity probe based on actinoallolide A to investigate its biological mode of action. This will allow ongoing labelling studies to identify their protein binding target(s).

Introduction

Among communicable illnesses, parasitic diseases are the fourth largest cause of mortality worldwide, being responsible for over 500 000 deaths in 2015.[1,2] Two such conditions are the neglected tropical diseases human African trypanosomiasis (sleeping sickness)[3–5] and Chagas disease,[6–10] both caused by protozoan parasites of the genus *Trypanosoma*. These illnesses are estimated to account for a loss of 455 000 disability-adjusted life years annually.[11] Trypanosomes are extremely adept at evading the immune system, and these neglected tropical diseases can only be cleared from the body with the help of chemotherapeutic agents.[12] However, the ongoing development of effective pharmaceutical agents against the causative agents of these diseases has been challenging due to two major factors.[13,14] First, the eukaryotic nature of protozoan parasites means that trypanosomes are biologically more closely related than bacteria to human cells. This renders the development of selective anti-trypanosomal drugs more challenging.[15] Secondly, as these diseases mainly affect less economically developed countries, a lack of financial incentive to develop new drugs has led to an urgent need for better, more effective and safer treatments for these neglected diseases.[16]

Fortunately, the natural world possesses a rich and structurally diverse source of antiparasitic compounds.[17] The actinoallolides (Fig. 1), a family of novel polyketides, are one such example, isolated by Iwatsuki and co-workers from a cultured strain (MK10-036) of the actinomycete bacterium *Actinoallomurus fulvus*, obtained from the roots of *Capsicum*

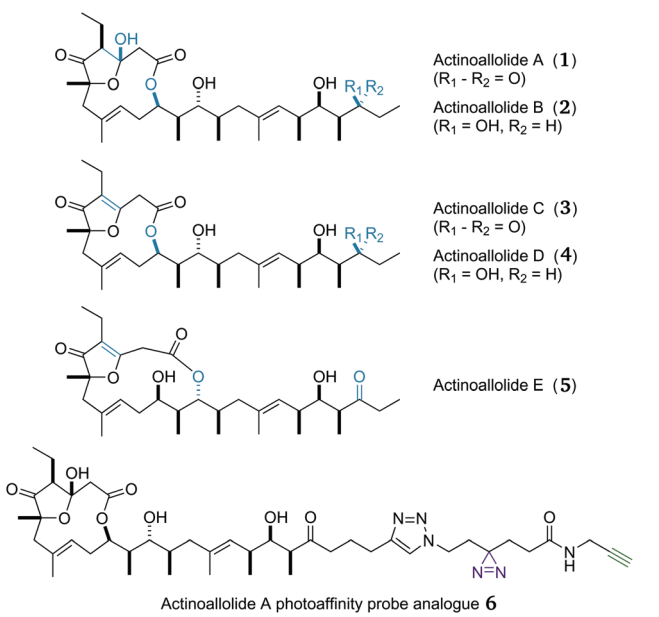

Fig. 1 3D structures of the five actinoallolide congeners **1–5** and the designed photoaffinity probe analogue **6**.

University Chemical Laboratory, University of Cambridge, Lensfield Road, CB2 1EW, UK

† Electronic supplementary information (ESI) available: Full experimental details and characterisation of new compounds, together with NMR comparisons of the synthetic and natural actinoallolides. See DOI: 10.1039/D0OB01831G

fruitescens collected in Thailand.[18] The 3D structure of actinoallolide A (**1**) was determined by spectroscopic analysis and X-ray crystallography, which revealed the presence of 10 stereocentres, two trisubstituted alkenes and a 12-membered macrolactone incorporating a five-membered hemiacetal. In addition, the structures of actinoallolides B–E (**2–5**) were confirmed by chemical correlation with actinoallolide A.

The actinoallolides were tested against three strains of *Trypanosoma* and compared with several commonly used antitrypanosomal drugs. Actinoallolides A–E were also tested for biological activity against *Trypanosoma brucei brucei*, the strain responsible for animal trypanosomiasis (Nagana disease) and compared with three of the most commonly used drug treatments. They all compared favourably, with actinoallolide A determined as the most potent by two orders of magnitude, with an IC_{50} of 8.3 nM. Actinoallolide A (**1**) was also tested against *Trypanosoma brucei rhodesiense*, a strain responsible for human African trypanosomiasis and *Trypanosoma cruzi*, the causative agent of Chagas disease, showing double the potency of benznidazole. Actinoallolide A (**1**) showed no observable activity against MRC-5 human cells, giving it a high selectivity index (>20 000).[19] It was inactive against Gram-positive and negative bacteria and against yeast and fungi, indicating a highly specific mechanism of antitrypanosomal activity that is yet to be determined.

The isolation group have also identified the actinoallolide biosynthetic gene cluster, proposed a biosynthesis,[20] and reported preliminary synthetic studies.[21] Herein, we give a full account of the first total synthesis of the actinoallolides,[22] which was enabled by a challenging ring-closing metathesis reaction to form the macrocyclic trisubstituted alkene, the most complex example of its kind.[23] As the biological target and mechanism of action of the actinoallolides are unknown, we sought to leverage our total synthesis to shed light on these unanswered questions. Based on a highly efficient endgame, we now report the design and synthesis of the actinoallolide A-based probe **6** for target identification using photoaffinity labelling.[24,25]

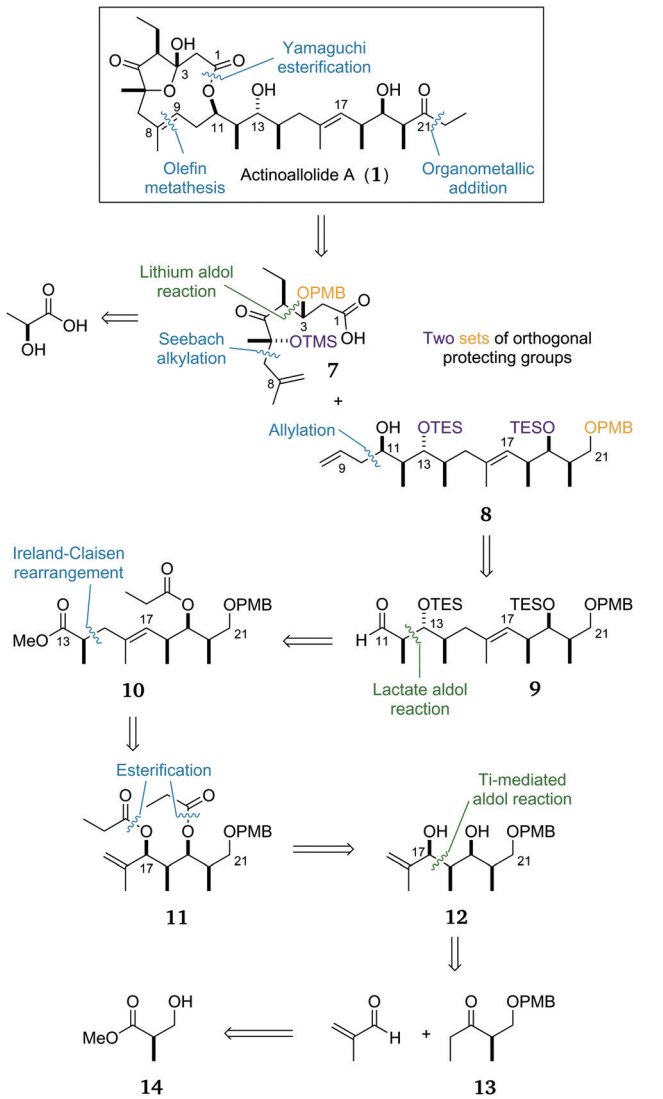

Scheme 1 Initially proposed retrosynthesis of actinoallolide A with the three key aldol reactions highlighted in green.

Results and discussion

Retrosynthetic analysis of actinoallolide A

Our proposed key bond disconnections (Scheme 1) were of the C_1 ester and the C_8–C_9 alkene to form two fragments of roughly equal size and complexity: the macrocycle precursor **7** and the side chain **8**. A major advantage of this approach is that it allows a flexible fragment coupling strategy whereby the two coupling steps could be undertaken in either order; cross metathesis could be followed by macrolactonisation, or esterification could be followed by ring-closing metathesis as desired.

The C_1–C_8 fragment **7** would be forged from natural (*S*)-lactic acid with key bonds formed *via* a Seebach alkylation and a diastereoselective aldol reaction. Protection of the C_3 and C_6 alcohols would allow late-stage unmasking of the delicate five-membered hemiacetal after deprotection and oxidation at C_3 to give actinoallolide A.

The side chain contains two distinct stereoclusters. The C_{11}–C_{14} stereotetrad was envisaged to be constructed by a substrate-controlled allylation of **9** preceded by a lactate aldol reaction to reveal, after redox adjustment, ester 10. The isolated C_{14} stereocentre in **10** could then be installed by an Ireland–Claisen rearrangement from the diester **11**. The 'all *syn*' stereotetrad in **12** can then be formed by a titanium-mediated aldol reaction/*in situ* reduction between methacrolein and ethyl ketone **13**, itself synthesised in three steps from (*R*)-Roche ester (**14**). The decision to attach the terminal ethyl group at such a late stage was made in order to form the C_{21} ketone as late as possible to facilitate late-stage diversification. A more complex organometallic reagent could be used to add any modified tail in place of the ethyl group.

Finally, the decision to utilise two sets of orthogonal protecting groups was informed by our planned endgame. The hydroxyl groups at C_{21} and C_3 require oxidation, whereas those at C_6, C_{13} and C_{19} do not. Thus it was planned to use benzyl ether-based groups for the former and silyl ethers for the latter hydroxyl groups.

Synthesis of the C_9–C_{21} side chain fragment (8)

The synthesis of side chain fragment **8** commenced with ethyl ketone **13**.[26] In previous work, the 'all-*syn*' aldol selectivity required for the construction of **12** had been achieved by use of tin(II) triflate as a Lewis acid.[27,28] While effective, the use of tin(II) triflate was procedurally cumbersome, especially on scale owing to its capricious preparation. We sought to improve upon this process by combining two recent developments in aldol chemistry. Romea and Urpí have reported the use of titanium Lewis acids for the highly selective aldol reactions of protected β-hydroxy ketones[29] and α-hydroxy ketones with an *in situ* reduction to afford the *syn*-1,3-diol.[30] It was reasoned that combining these two processes would afford the desired 'all-*syn*' stereotetrad in diol **12**. In the event, application of this *in situ* reduction with $LiBH_4$ to the aldol addition of ketone **13** and methacrolein provided diol **12** in 90% yield as a single diastereomer (Scheme 2). Owing to the oxophilicity of the titanium and boron complexes formed in the reaction, an extended workup incorporating treatment with hydrogen peroxide and multiple washings with Rochelle salt solution was found to be necessary for release of **12**.

After selective monoesterification of the allylic alcohol in diol **12** was found to be problematic, it was decided to proceed through the required Ireland–Claisen rearrangement[31] with diester **11**. Only the O_{17} ester was correctly positioned to undergo the [3,3]-sigmatropic rearrangement while the O_{19} ester would be removed during the later reduction of the C_{13} methyl ester to the aldehyde. Guided by a similar Ireland–Claisen rearrangement used in the total synthesis of ebelactone,[32] we began investigating this key step. Initial attempts at performing this reaction led to appreciable formation of the C_{14} α-silylated by-product. This TMS group could be removed with K_2CO_3 in MeOH but, as would be expected, led to significant epimerisation. The epimer was visible by NMR and provided evidence that the Ireland–Claisen product had been obtained as a single diastereomer. This side reaction is proposed to occur *via* enolisation of the formed silyl ester by excess LDA and trapping of this enolate with TMSCl. As such, it was important to precisely control the equivalents of LDA used. In order to avoid quenching any LDA, it is necessary to remove all traces of HCl from the large excess of TMSCl used. In the ebelactone work, this was accomplished by premixing TMSCl with Et_3N and centrifuging the resulting suspension to remove the precipitate. In this work, removal of the precipitate was more conveniently accomplished *via* filtration through a syringe tip filter (PVDF membrane, 0.45 μm pores). Optimising the quantity of LDA used increased the yield to 73% with no observable formation of the α-silylated by-product. For ease of isolation, the carboxylic acid product was methylated without purification to afford methyl ester **10**.

Pleasingly, the DIBAL-H reaction of this ester **10** proceeded well, reducing the methyl ester at C_{13} to the corresponding aldehyde and liberating the free hydroxyl group at C_{19}, setting the stage for the second strategic aldol reaction. While substrate control was used to construct all other stereocentres in side chain fragment **8**, the anticipated mismatch between the Felkin–Anh selectivity of aldehyde **15** and the desired configuration at the C_{13} hydroxyl stereocentre made it impossible in this case. Using boron aldol methodology developed in the group,[33,34] we were able to couple aldehyde **15** with lactate-derived ketone **16** to form *anti* adduct **17** as a single diastereomer, overriding the inherent facial selectivity of aldehyde **15** to install the C_{12} and C_{13} stereocentres. Protection of both

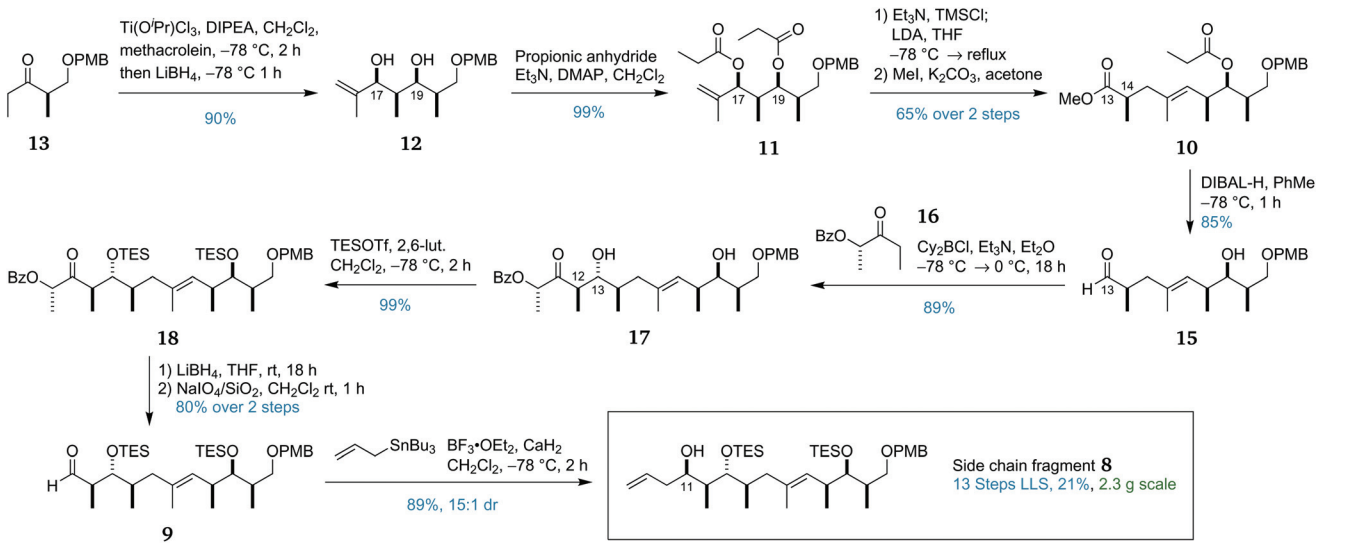

Scheme 2 Synthesis of the side chain fragment **8**.

hydroxyl groups as TES ethers then afforded **18** which underwent a standard two-step auxiliary removal procedure to provide aldehyde **9**.[33] Addition of the allyl moiety to **9** to complete the side chain fragment **8** required some optimisation with the use of allylmagnesium chloride or allyltrimethylsilane leading to low diastereoselectivity. Fortunately, it was found that the utilisation of allyltributylstannane in a Hosomi–Sakurai reaction[35,36] with the non-chelating Lewis acid $BF_3{\cdot}OEt_2$ afforded **8** in high yield with 15 : 1 dr.

This completed the scalable and high-yielding synthesis of the side chain fragment **8** in 13 linear steps from (*R*)-Roche ester (**14**) with an overall yield of 21%. This excellent yield (an average of 89% per step) and the scalability of the route allowed 2.3 g to be prepared, providing ample material for development of the endgame.

Synthesis of the C_1–C_8 macrocycle precursor fragment

The synthesis of the macrocycle precursor fragment began with the construction of dioxolanone **19** *via* a two-step procedure (Scheme 3),[37] allowing an enolate alkylation[38] with methallyl bromide to install the C_6 stereocentre. This reaction proved difficult to optimise, with a 53% yield of **20**, albeit as a single diastereomer. This was due to formation of a major by-product due to self-reaction of the dioxolanone.[39] However, the modest yield was deemed sufficient and allowed the preparation of **20** on a multi-gram scale.

The removal of the pivaldehyde-derived auxiliary *via* ring opening of dioxolanone **20** was the next task to be accomplished. In preliminary studies, the desired conversion to propyl ketone **22** was achieved using a four-step sequence commencing with ring opening to the methyl ester. We envisaged abridging this sequence by using a different ring-opening procedure. The first attempt to convert the dioxolanone to the propyl ketone directly by addition of propylmagnesium bromide, however, was unsuccessful, yielding either unreacted starting material or the double addition product. Ring opening to the Weinreb amide **21** was trialled next and proceeded in excellent yield using the *in situ* generated anion of *N*,*O*-dimethylhydroxylamine. With this result, a one-pot conversion to the desired propyl ketone was examined. However, the conversion of **21** to the corresponding propyl ketone *in situ* proved unsuccessful even with warming to room temperature. Weinreb amide **21** was next silyl protected and converted to propyl ketone **22**, required for the planned C_3–C_4 bond-forming lithium-mediated aldol reaction. As the protecting group strategy utilised a silyl group at C_6 and a PMB group at C_3, the C_1 protecting group was required to be orthogonal to both.

From propyl ketone **22**, two routes to macrocycle precursor fragment **7** were initially considered. The first plan was to utilise an orthoester protecting group on aldehyde **23**, as this would allow access to C_1 at the desired carboxylic acid oxidation level. This lithium-mediated aldol reaction afforded *syn* adduct **24**, providing the desired diastereomer in good yield and with useful diastereoselectivity. We had planned to protect the C_3 alcohol with a PMB group, however all attempted conditions led to no reaction or to degradation, presumably owing to steric congestion. Furthermore, removal of the orthoester protecting group could not be achieved without degradation due to the acid and base sensitivity of the aldol adduct.

With this approach proving to be unviable, C_1 was next introduced at the protected alcohol oxidation state. Noting that PMB groups can be oxidatively transposed,[40] this second plan was to utilise a PMB group on aldehyde **25** to produce

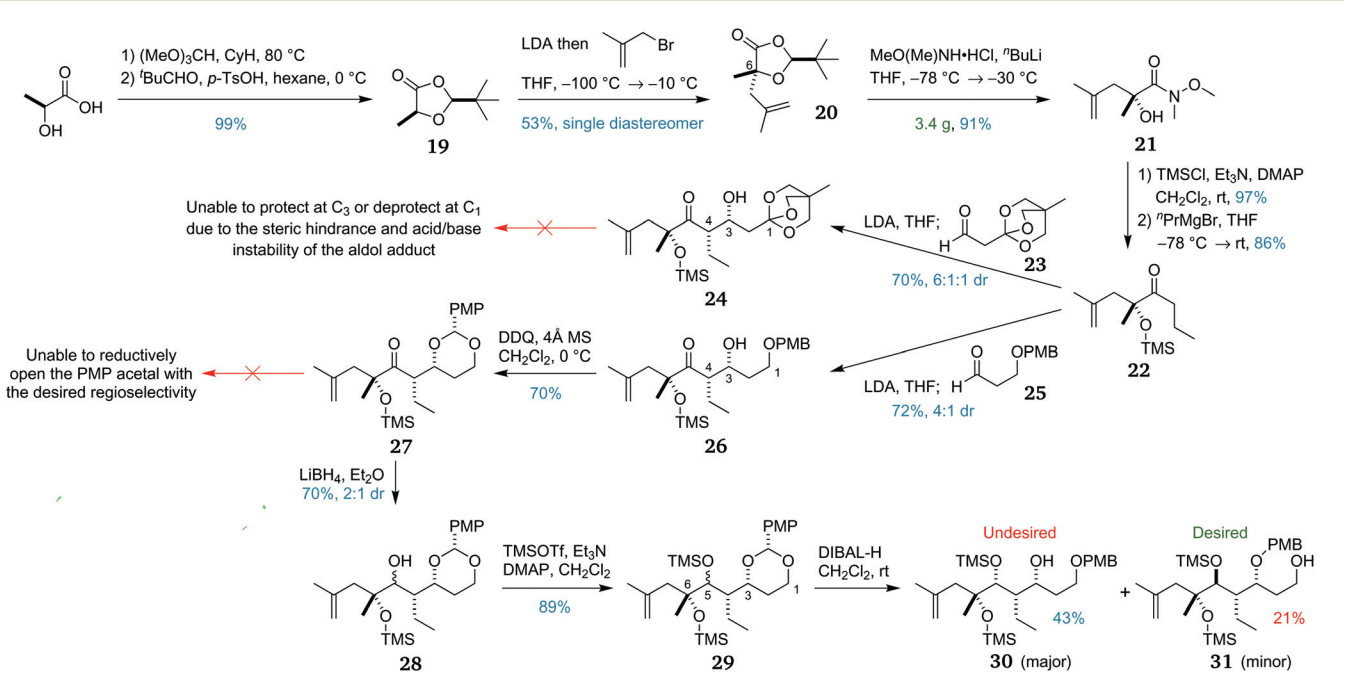

Scheme 3 Synthesis of the key propyl ketone **22** and attempts at elaboration.

aldol adduct **26**. As before, the lithium-mediated aldol reaction afforded the *syn* adduct in good yield, in a 4 : 1 ratio of diastereomers. The major diastereomer was then converted to PMP acetal **27** by treatment with DDQ under anhydrous conditions. Disappointingly, subsequent attempts at reductive PMP opening to the primary alcohol were all unsuccessful, with the use of DIBAL-H[40] or $NaCNBH_3$/TMSCl[41] causing side-reactions or reacting with the undesired regioselectivity to revert to secondary alcohol **26**. This unexpected selectivity may be due to preferential chelation of the Lewis acid between the C_3 oxygen and the ketone rather than the less hindered C_1 oxygen as would normally be expected.

Given that this selectivity problem was likely due to the propensity of the C_5 ketone to coordinate with the adjacent C_3 oxygen, it was proposed that reducing the C_5 ketone and transiently protecting the resulting alcohol as a TMS ether might circumvent this impasse. Ketone **27** was thus reduced using $LiBH_4$ to form secondary alcohol **28** in 70% yield and 2 : 1 dr. The diastereomers were inseparable by chromatography so the alcohols were then silylated to form **29**. This mixture of diastereomeric PMP acetals then underwent reductive opening with DIBAL-H. Surprisingly, the two epimeric acetals reacted with opposing regioselectivities, with the major diastereomer forming the undesired secondary alcohol **30** and the minor diastereomer forming the desired primary alcohol **31**.

In light of this mixed result, it was reasoned that if we could override the inherent substrate selectivity of ketone **27** to reduction, and obtain the 1,3-*anti* diastereomer selectively, this might provide a viable route to the macrocycle fragment. Testing a range of simple reducing agents was fruitless, with each one either giving the undesired selectivity or no reaction. It was next decided to attempt the reduction of the C_5 ketone prior to PMP acetal formation, using the C_3 alcohol in **26** to direct a 1,3-*anti* Evans–Tishchenko[42] or Evans–Saksena reduction.[43] With prolonged reaction time and an excess of the samarium catalyst,[42] it was possible to achieve a low yield of 10% with 2 : 1 dr for the former reaction, but no product was obtained under the latter conditions. This was attributed to the steric hindrance of the C_5 ketone with its quaternary α stereocentre incorporating a bulky OTMS group.

These frustrations *en route* to the macrocycle precursor fragment led us to consider more substantial modifications to the route. The efforts thus far had focused on installing a PMB protecting group at C_3, either by a 'PMB transposition'of the PMB group at C_1, or by direct protection of the alcohol at C_3. The former method had failed due to the selectivity problems with opening the intermediate PMP acetal and the latter had failed due to the steric hindrance of aldol adduct **26** and its instability under forcing conditions. To circumvent these problems within the constraints of the overall protecting group strategy – that is to allow for the chemoselective oxidative removal of the C_3 and C_{21} protecting groups in one operation, it was proposed to switch the C_3 protecting group from PMB to PMBM (*para*-methoxybenzyloxymethyl).[44] Like the PMB group, it can be oxidatively removed orthogonally to silyl groups but can be installed under far milder conditions. However, as the PMBM group was liable to cleavage under oxidative conditions, this alteration necessitated a revision of the C_1 protecting group such that it could be removed orthogonally to the PMBM group. Given that the aromatic ring in the DMB (3,4-dimethoxybenzyl)[45] group is more electron rich than in the PMBM group, it was anticipated that selective oxidative cleavage of the DMB group would be possible.[46]

The corresponding DMB-protected aldehyde **32** required for the aldol coupling was prepared *via* a three-step procedure.[47] This aldehyde then underwent an analogous lithium-mediated aldol reaction with propyl ketone **22**, providing *syn* adduct **33** (Scheme 4) in similar yield and dr to that obtained from the PMB-protected variant. This was subsequently PMBM protected using the mild base DIPEA in refluxing acetonitrile overnight to afford PMBM ether **34** in excellent yield. With triply-protected aldol adduct **34** in hand, selective DMB cleavage was next attempted. Fortunately, one equivalent of DDQ with careful monitoring afforded primary alcohol **35** in excellent yield, with complete retention of the PMBM group. This then underwent a double oxidation sequence; first was a Swern oxidation to give aldehyde **36**, then a Pinnick oxidation provided the complete macrocycle precursor fragment **37**.

Overall, macrocycle precursor fragment **37** was synthesised in 10 linear steps from (*S*)-lactic acid with an overall yield of

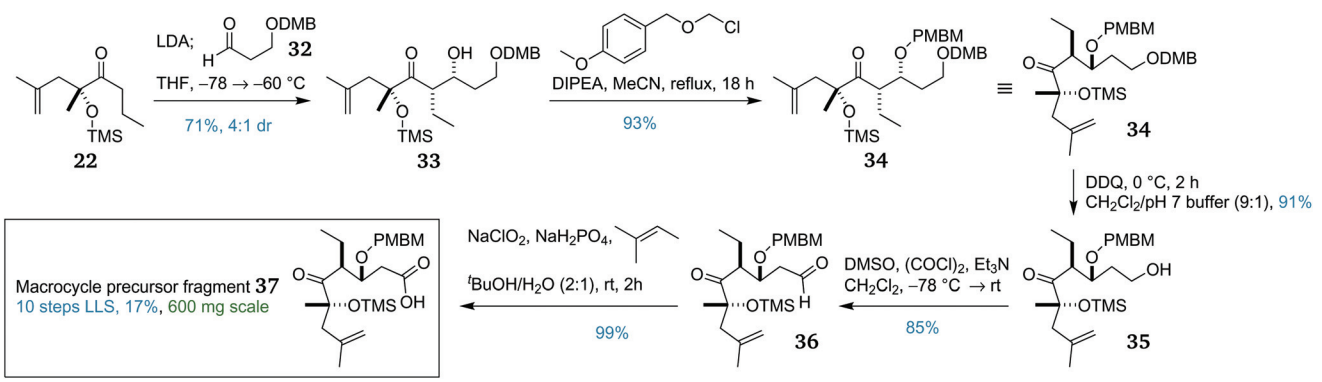

Scheme 4 Completion of the synthesis of macrocycle precursor fragment **37**.

17%. This represents an average of 84% per step, and the scalability of the route allowed 600 mg to be prepared, providing ample material for development of the endgame.

Fragment union and endgame

With key fragments **8** and **37** in hand, the stage was set to explore the pivotal fragment union sequence. The retrosynthetic plan (Scheme 1) had left the ordering of these steps flexible. However, preliminary investigations had indicated that an efficient and stereoselective cross metathesis to give the trisubstituted 8*E* alkene was unlikely to succeed, so we proceeded with exploring the esterification/RCM sequence. The fragments **37** and **8** were coupled together under standard Yamaguchi conditions[48] to afford ester **38** in an excellent yield of 99%, enabling investigation of the "do-or-die" macrocycle-forming RCM step (Scheme 5).

The first attempt at cyclisation of **38** using Grubbs second-generation catalyst (G-II)[49,50] in refluxing degassed CH_2Cl_2 provided only the undesired dimer **40** in quantitative yield (Table 1, entry 1). Increasing the catalyst loading to 50 mol% (entry 2) or the use of higher-boiling solvents (entries 3 and 4) failed to provide any macrocyclic product, in each case returning only dimer **40**. As an additional measure, a solution of catalyst was added portionwise over the initial few hours of the reaction to reduce catalyst decomposition, although the colour change from purple to brown was observed within 30 min of each addition, indicating rapid catalyst degradation. In light of these failures, we switched to the more reactive Hoveyda–Grubbs second-generation catalyst (HG-II).[51,52] Gratifyingly, an initial RCM reaction of **38**, overnight in refluxing toluene, afforded an inseparable 1 : 1 mixture of dimer **40** and desired macrocycle **39** (entry 5). Increasing the catalyst loading to 40 mol% and the reaction time to 72 h increased the product : dimer ratio to 1.5 : 1 (entry 6). In an attempt to increase the reaction rate and yield, the solvent was changed to *o*-xylene to allow reflux at a higher temperature. Surprisingly, this led to a reduction in the product : dimer ratio to 1.2 : 1 (entry 9), indicating that there was a 'sweet spot' temperature at around 110–140 °C, below which the reaction is prohibitively slow and above which catalyst decomposition occurs.

By this point, a mechanistic hypothesis was proposed whereby the terminal alkene present in **38** rapidly dimerises. The ruthenium catalyst can then reinsert into the new disubstituted alkene in this dimer and can then undergo one of two processes. In most cases, this undergoes an intermolecular reaction with another molecule of dimer **40** to reversibly return to the dimer. Much more slowly, but irreversibly, this ruthenium carbene can undergo an intramolecular reaction with the 1,1-disubstituted alkene to afford desired macrocycle **39**. To help encourage the slow, irreversible RCM step, the duration of the reaction was increased to seven days, increasing the product : dimer ratio to 3 : 1 and providing the desired product with an improved yield of 75% (entry 10). To our knowledge, this challenging and remarkable transformation is the most complex example of an RCM reaction to form a trisubstituted alkene in a medium-sized ring.[23]

Table 1 Screening of ring-closing metathesis conditions for the formation of macrocycle **39** from precursor **38** (G-II = Grubbs second-generation catalyst, HG-II = Hoveyda–Grubbs second-generation catalyst)

Entry	Cat. (mol%)	Solvent (mM)	Temp.	Time	39 : 40
1	G-II (20)	CH_2Cl_2 (5)	40 °C	18 h	0 : 1
2	G-II (50)	CH_2Cl_2 (10)	40 °C	18 h	0 : 1
3	G-II (20)	Benzene (1)	80 °C	18 h	0 : 1
4	G-II (20)	Toluene (1)	110 °C	18 h	0 : 1
5	HG-II (20)	Toluene (1)	110 °C	18 h	1 : 1
6	HG-II (40)	Toluene (1)	110 °C	72 h	1.5 : 1
7	HG-II (40)	Toluene (10)	110 °C	72 h	1.3 : 1
8	HG-II (40)	Toluene (0.25)	110 °C	72 h	2 : 1
9	HG-II (40)	Xylene (0.25)	145 °C	72 h	1.2 : 1
10	HG-II (40)	Toluene (1)	110 °C	7 d	3 : 1

Having prepared an abundant supply of advanced intermediate **39**, the removal of both PMB-containing protecting groups was accomplished by treatment with DDQ, affording diol **41** in 94% yield (Scheme 6). Chemoselective oxidation of the primary alcohol at C_{21} in the presence of the C_3 secondary alcohol was achieved using a TEMPO/BAIB oxidation[53,54] which afforded aldehyde **42** in 90% yield. Subsequently, chemoselective addition of ethylmagnesium bromide to the newly formed aldehyde in the presence of the C_5 ketone proceeded smoothly, affording an inseparable epimeric mixture of **43** in 91% yield, with no observable attack at the ketone.

Having completed the full carbon backbone of the actinoallolides, our attention now turned to the final two steps of oxidation and global deprotection. Oxidation of both secondary alcohols at C_3 and C_{21} was initially attempted under Swern conditions, however, this was found to be unreliable. Alternatively, the oxidation was performed using the milder Dess–Martin periodinane.[55] Double oxidation under these conditions was found to be clean and reliable, providing triketone **44** in 99% yield.

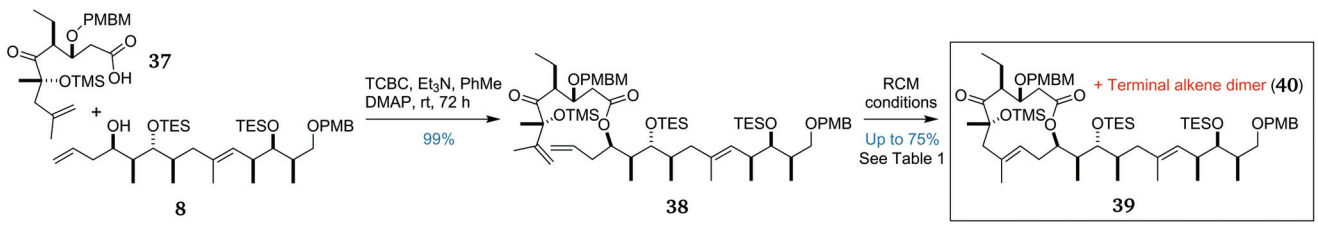

Scheme 5 Fragment union and RCM-mediated formation of the 12-membered macrocycle **39**.

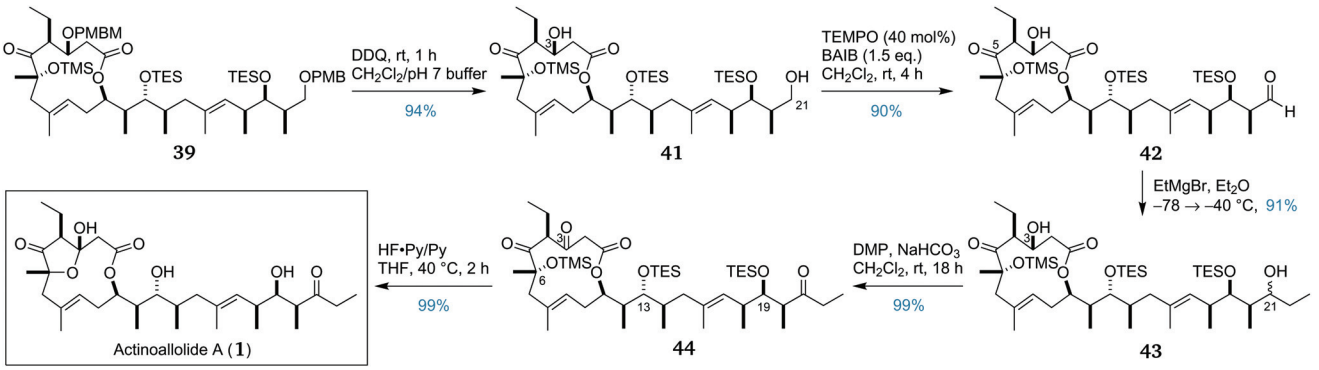

Scheme 6 Endgame and completion of the total synthesis of actinoallolide A (**1**).

The only obstacle now remaining was the final deprotection. The conditions should ensure complete cleavage of the C_6 TMS ether and the C_{13} and C_{19} TES ethers, while also forming the transannular hemiacetal. The conditions were also required to be sufficiently mild to avoid any possible deleterious side reactions. Preliminary experience with the lability of the hemiacetal motif led to the hypothesis that actinoallolides C–E may be artefacts of the elaborate chromatographic isolation process. Consequently, we were particularly cautious to avoid elimination across the C_3–C_4 bond and transesterification of the macrolactone in **44**. Initial attempts using TBAF were unsuccessful, leading either to incomplete deprotection or degradation. Pleasingly, acidic fluorous deprotection conditions proved successful, with treatment of **44** with a 1 : 3 mixture of HF·py/py with warming to 40 °C effecting quantitative conversion to (+)-actinoallolide A (**1**). The resulting synthetic actinoallolide A possessed comparable specific rotation and identical NMR spectra to those of the natural product (see the ESI†).

The total synthesis of (+)-actinoallolide A (**1**) was thus achieved in 20 linear steps from (*R*)-Roche ester (**14**) with an overall yield of 8%, representing an average yield of 88% per step. Importantly, this first total synthesis gave an orthogonal validation of the full 3D structure and absolute configuration of actinoallolide A and will enable further biological investigations of this highly potent family of natural products.

Conversion of actinoallolide A to actinoallolides B–E

We next sought to access the other four congeners, actinoallolides B–E (**2**–**5**), by replication of the conversion protocols in the isolation paper (Scheme 7).[18] Actinoallolide A (**1**) underwent a 1,3-*syn* hydroxyl-directed reduction using triethylborane followed by sodium borohydride to afford actinoallolide B (**2**) in 93% yield and as a single diastereomer. Subsequent treatment of actinoallolide B (**2**) with trifluoroacetic acid caused dehydration of the cyclic hemiacetal to provide actinoallolide D (**4**) in 99% yield.

During the initial purification of actinoallolide A using silica chromatography, some minor by-product formation was observed. Using alumina instead, attempted purification of actinoallolide A led to conversion to a 1 : 1 mixture of actinoallolide C (**3**) and actinoallolide E (**5**). This unexpected result indicated the instability of the cyclic hemiacetal moiety to basic conditions, perhaps explaining why global deprotection was unsuccessful under basic fluorous conditions. This spontaneous conversion of actinoallolide A (**1**) to actinoallolides C (**3**) and E (**5**) on alumina also provides evidence that these compounds are isolation artefacts rather than genuine natural products. This serendipitous result completed our synthesis of all five members of the actinoallolides.

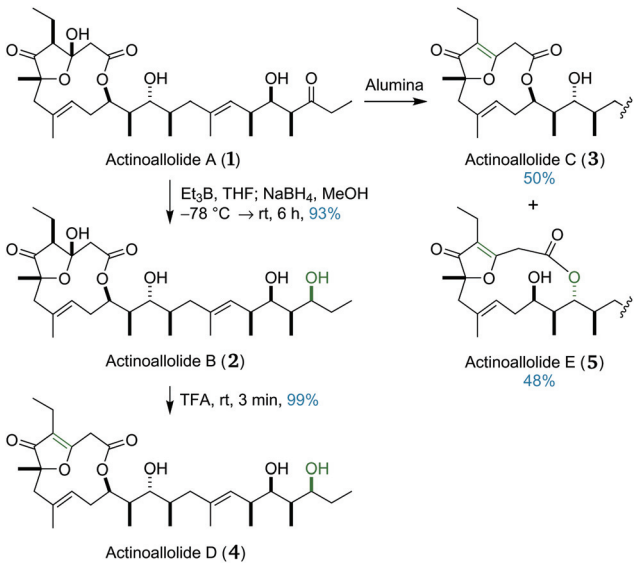

Scheme 7 Conversion of actinoallolide A (**1**) to actinoallolides B–E (**2**–**5**).

Based on the assumption that actinoallolides C and E are isolation artefacts, it is likely that actinoallolide D is also an artefact, arising from dehydration of actinoallolide B. This would leave actinoallolides A and B as the only true natural products, differing only in the oxidation level at C_{21}. In examining the proposed biosynthesis of actinoallolide A,[20] the authors had identified an inactive ketoreductase domain (KR1) in the polyketide synthase responsible for the biosynthesis of actinoallolide A. They commented that "although KR1 has catalytic amino acids and the NADPH binding motif, it seems

to be inactive, as predicted from the structure of actinoallolide A that has a ketone at C_{21}". If, rather than being inactive, the KR1 domain were instead partially active, this identified polyketide synthase would be able to generate both actinoallolides A and B. When the KR1 domain performs the C_{21} reduction, actinoallolide B, containing the C_{21} alcohol, is produced, and when transfer to module 2 occurs before the reduction can take place, the product is instead actinoallolide A, with the unreduced C_{21} ketone. On inspection of the amino acid sequence of the KR1 domain, it possesses both sets of characteristic amino acids which determine whether reduction affords the L- or D-configuration, potentially explaining its partial inactivity.

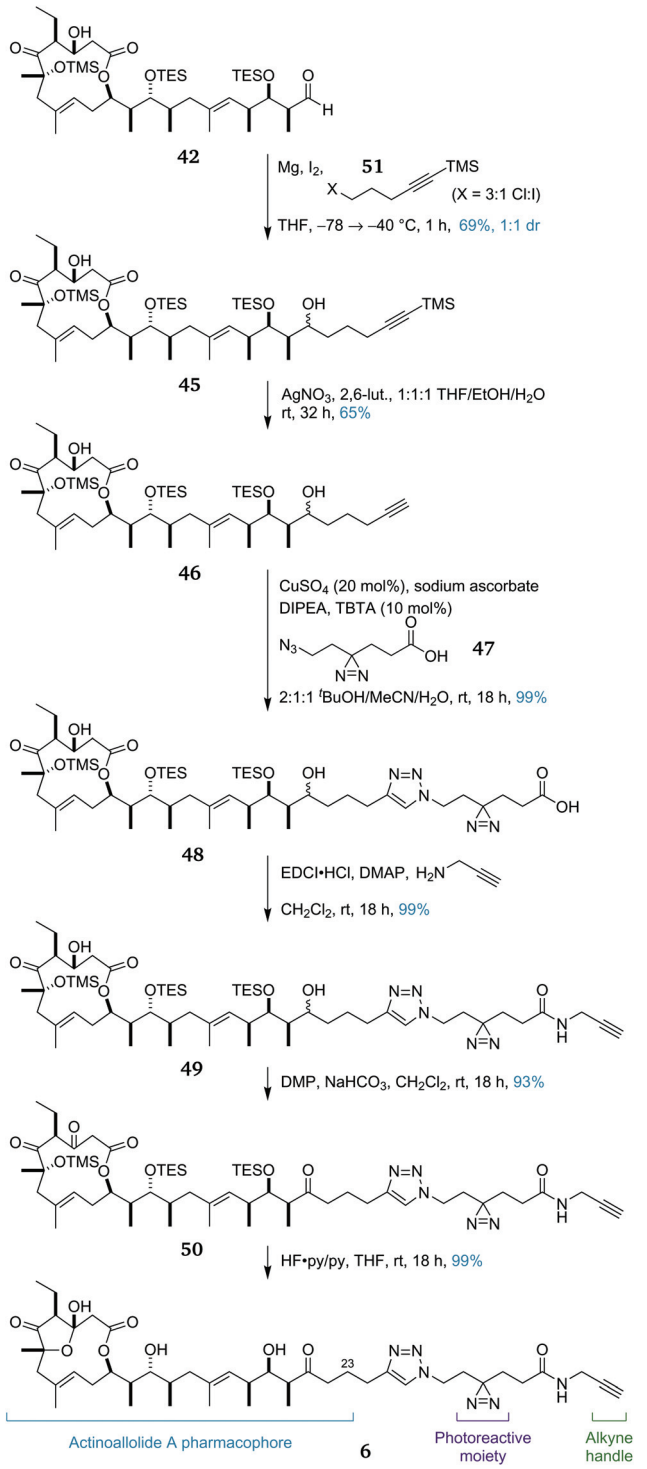

Scheme 8 Diversion of advanced intermediate **42** towards the synthesis of photoaffinity probe analogue **6** of actinoallolide A.

Synthesis of an actinoallolide A photoaffinity probe analogue

Having achieved a practical, convergent and high-yielding total synthesis of the actinoallolides, we moved onto the design and synthesis of a photoaffinity probe analogue (Scheme 8) to identify their biological target. In order to minimally perturb the structure of the native natural product, the photoaffinity probe **6** was chosen to extend from the C_{23} terminus.[56] The photoreactive moiety is a diazirine, decomposing to a highly-reactive carbene upon irradiation at 365 nm, facilitating cross-linking to the bound target protein. The functional handle is a terminal alkyne, allowing the facile conjugation of any desired reporter tag using a copper-catalysed azide–alkyne cycloaddition.[25]

The synthesis of probe **6** began by intercepting the advanced intermediate **42**. In the total synthesis, addition of an ethyl group was required to complete the actinoallolide carbon skeleton. Instead, the addition of the Grignard reagent derived from halide **45** afforded diol **46** in 69% yield as an inconsequential 1 : 1 mixture of diastereomers. Chemoselective removal of the alkynyl TMS group was achieved by treatment with $AgNO_3$ and gave **47** in 65% yield. Next, a copper-catalysed azide–alkyne cycloaddition between alkyne **47** and linker fragment **48** (prepared from 1,4-cylohexanedione in eight steps)[57] proceeded to afford triazole **49** (99%).

The EDCI/DMAP-mediated amidation of **49** with propargylamine proceeded smoothly, affording amide **50** in 99% yield. This amide then underwent a double DMP-mediated oxidation to afford triketone **51** (93%). Finally, global deprotection under acidic fluorous conditions proceeded with an excellent yield of 99%, cleaving all three silyl ethers and inducing formation of the transannular five-membered hemiacetal to form photoaffinity probe **6**. To date, this route has provided 26 mg of **6**, sufficient material for the required photoaffinity experiments. In preliminary studies, the biological activities of synthetic actinoallolide A (**1**) and photoaffinity probe **6** have been confirmed and photoaffinity studies are currently ongoing.

Conclusions

This account details the first total synthesis of the actinoallolides, a family of polyketide natural products prized for their promising anti-trypanosomal properties.[58] This feat has been accomplished in a scalable, high-yielding and stereoselective fashion, giving actinoallolide A (**1**) in 20 linear steps from (*R*)-Roche ester (**14**) with an overall yield of 8%. This was achieved in a highly convergent manner, utilising two fragments **8** and

37 of similar complexity, which were obtained in 13 and 10 steps respectively. The stubbornness of C_3 manipulation to standard 'PMB transposition' conditions was frustrating and necessitated modifications to the original strategy. Fortunately, the judicious choice of alternative protecting groups allowed us to overcome this obstacle.

Fragment union was accomplished by esterification followed by a highly challenging ring-closing metathesis, gratifyingly forming the macrocyclic trisubstituted alkene as a single geometrical isomer. This "do-or-die" transformation required significant optimisation and is the most complex example of its kind. A high-yielding endgame finally afforded actinoallolide A. Actinoallolide A was then converted to actinoallolides B–E, completing the total synthesis of the entire natural product family. The alumina-mediated conversion of actinoallolide A to actinoallolides C and E provides evidence that actinoallolides C–E are isolation artefacts, with actinoallolides A and B as the only true natural products. On review of the biosynthetic data for the actinoallolides, a partially active ketoreductase domain in the actinoallolide A polyketide synthase has been postulated to be responsible for generating these two congeneric natural products.

With the secondary aim of probing how actinoallolide A exerts its highly specific biological effects, this route was diverted to give **6** as a designed photoaffinity probe. This was achieved in six steps from advanced intermediate **42**. Ongoing work is focused on using **6** in various assays with the aim of identifying the biological target of actinoallolide A. Identification of this target and knowledge of the mechanism of action may allow the generation of simplified, more synthetically tractable or more potent actinoallolide analogues in the ongoing effort to develop new, effective medicinal agents to treat neglected tropical diseases.

Conflicts of interest

There are no conflicts to declare.

Acknowledgements

We thank the Herchel Smith Fund (studentship to M. J. A.), Dr Rachel J. Porter and Dr Simon Williams for assistance, and Thomas Hayhow (AstraZeneca) for his interest. We are grateful to Professor Terry Smith and Dr Gordon Florence at the University of St Andrews for performing the preliminary bioactivity assays. We also acknowledge the National Mass Spectrometry Facility at Swansea University.

References

1 C. Mathers, G. Stevens, W. R. Mahanani, J. Ho, D. M. Fat and D. Hogan, *Global Health Estimates* 2015*: Deaths by Cause, Age, Sex, by Country and by Region*, 2000-2015, World health organization technical report, 2016.
2 P. J. Hotez and A. Kamath, *PLoS Neglected Trop. Dis.*, 2009, **3**, e412.
3 P. Büscher, G. Cecchi, V. Jamonneau and G. Priotto, *Lancet*, 2017, **390**, 2397–2409.
4 R. Brun, J. Blum, F. Chappuis and C. Burri, *Lancet*, 2010, **375**, 148–159.
5 *Trypanosomes and Trypanosomiasis*, ed. S. Magez and M. Radwanska, Springer-Verlag, Wien, 2014.
6 J. Bermudez, C. Davies, A. Simonazzi, J. P. Real and S. Palma, *Acta Trop.*, 2016, **156**, 1–16.
7 J. A. Pérez-Molina and I. Molina, *Lancet*, 2018, **391**, 82–94.
8 C. Bern, *N. Engl. J. Med.*, 2015, **373**, 456–466.
9 J. D. Stanaway and G. Roth, *Global Heart*, 2015, **10**, 139–144.
10 P. J. Hotez, E. Dumonteil, L. Woc-Colburn, J. A. Serpa, S. Bezek, M. S. Edwards, C. J. Hallmark, L. W. Musselwhite, B. J. Flink and M. E. Bottazzi, *PLoS Neglected Trop. Dis.*, 2012, **6**, e1498.
11 WHO Disease burden and mortality estimates, http://www.who.int/healthinfo/global_burden_disease/estimates/en/, (accessed September 2020).
12 D. J. Barry and R. McCulloch, *Adv. Parasitol.*, 2001, **49**, 1–70.
13 M. C. Field, D. Horn, A. H. Fairlamb, M. A. J. Ferguson, D. W. Gray, K. D. Read, M. De Rycker, L. S. Torrie, P. G. Wyatt, S. Wyllie and I. H. Gilbert, *Nat. Rev. Microbiol.*, 2017, **15**, 217–231.
14 P. E. Cockram and T. K. Smith, *J. Nat. Prod.*, 2018, **81**, 2138–2154.
15 A. Strelkauskas, A. Edwards, B. Fahnert, G. Pryor and J. Strelkauskas, *Microbiology: A Clinical Approach*, Garland Science, 2015.
16 A. R. Renslo and J. H. McKerrow, *Nat. Chem. Biol.*, 2006, **2**, 701–710.
17 L. Paloque, A. Triastuti, G. Bourdy and M. Haddad, *Natural Antimicrobial Agents*, Springer International Publishing, Cham, 2018, pp. 215–245.
18 Y. Inahashi, M. Iwatsuki, A. Ishiyama, A. Matsumoto, T. Hirose, J. Oshita, T. Sunazuka, W. Panbangred, Y. Takahashi, M. Kaiser, K. Otoguro and S. Omura, *Org. Lett.*, 2015, **17**, 864–867.
19 B. L. Roth, *The Serotonin Receptors: From Molecular Pharmacology to Human Therapeutics*, Springer Science and Business Media, 2008.
20 Y. Inahashi, T. Shiraishi, A. Také, A. Matsumoto, Y. Takahashi, S. Omura, T. Kuzuyama and T. Nakashima, *J. Antibiot.*, 2018, **71**, 749–752.
21 J. Oshita, Y. Noguchi, A. Watanabe, G. Sennari, S. Sato, T. Hirose, D. Oikawa, Y. Inahashi, M. Iwatsuki, A. Ishiyama, S. Omura and T. Sunazuka, *Tetrahedron Lett.*, 2016, **57**, 357–360.
22 For a preliminary communication, see: M. J. Anketell, T. M. Sharrock and I. Paterson, *Angew. Chem.*, 2020, **59**, 1572–1576.
23 C. Lecourt, S. Dhambri, L. Allievi, Y. Sanogo, N. Zeghbib, R. B. Othman, M.-I. Lannou, G. Sorin and J. Ardisson, *Nat. Prod. Rep.*, 2018, **35**, 105–124.

24 E. Smith and I. Collins, *Future Med. Chem.*, 2015, **7**, 159–183.
25 L. B. Tulloch, S. K. Menzies, A. L. Fraser, E. R. Gould, E. F. King, M. K. Zacharova, G. J. Florence and T. K. Smith, *PLoS Neglected Trop. Dis.*, 2017, **11**, e0005886.
26 I. Paterson, G. J. Florence, K. Gerlach, J. P. Scott and N. Sereinig, *J. Am. Chem. Soc.*, 2001, **123**, 9535–9544.
27 I. Paterson, S. J. Fink, L. Y. W. Lee, S. J. Atkinson and S. B. Blakey, *Org. Lett.*, 2013, **15**, 3118–3121.
28 I. Paterson and R. D. Tillyer, *Tetrahedron Lett.*, 1992, **33**, 4233–4236.
29 J. G. Solsona, J. Nebot, P. Romea and F. Urpí, *J. Org. Chem.*, 2005, **70**, 6533–6536.
30 J. Esteve, S. Matas, M. Pellicena, J. Velasco, P. Romea, F. Urpí and M. Font-Bardia, *Eur. J. Org. Chem.*, 2010, 3146–3151.
31 R. E. Ireland and R. H. Mueller, *J. Am. Chem. Soc.*, 1972, **94**, 5897–5898.
32 I. Paterson and A. N. Hulme, *J. Org. Chem.*, 1995, **60**, 3288–3300.
33 I. Paterson and D. J. Wallace, *Tetrahedron Lett.*, 1994, **35**, 9087–9090.
34 I. Paterson, D. J. Wallace and C. J. Cowden, *Synthesis*, 1998, 639–652.
35 J. H. Lee, *Tetrahedron*, 2020, **76**, 131351.
36 A. B. Smith, T. J. Beauchamp, M. J. LaMarche, M. D. Kaufman, Y. Qiu, H. Arimoto, D. R. Jones and K. Kobayashi, *J. Am. Chem. Soc.*, 2000, **122**, 8654–8664.
37 R. Nagase, Y. Oguni, T. Misaki and Y. Tanabe, *Synthesis*, 2006, 3915–3917.
38 D. Seebach, R. Naef and G. Calderari, *Tetrahedron*, 1984, **40**, 1313–1324.
39 J. S. Kingsbury and E. J. Corey, *J. Am. Chem. Soc.*, 2005, **127**, 13813–13815.
40 G. Ehrlich, J. Hassfeld, U. Eggert and M. Kalesse, *J. Am. Chem. Soc.*, 2006, **128**, 14038–14039.
41 R. Johansson and B. Samuelsson, *J. Chem. Soc., Perkin Trans. 1*, 1984, 2371–2374.
42 D. A. Evans and A. H. Hoveyda, *J. Am. Chem. Soc.*, 1990, **112**, 6447–6449.
43 D. A. Evans, K. T. Chapman and E. M. Carreira, *J. Am. Chem. Soc.*, 1988, **110**, 3560–3578.
44 A. P. Kozikowski and J.-P. Wu, *Tetrahedron Lett.*, 1987, **28**, 5125–5128.
45 Y. Oikawa, T. Tanaka, K. Horita, T. Yoshioka and O. Yonemitsu, *Tetrahedron Lett.*, 1984, **25**, 5393–5396.
46 D. A. Evans, P. H. Carter, E. M. Carreira, A. B. Charette, J. A. Prunet and M. Lautens, *J. Am. Chem. Soc.*, 1999, **121**, 7540–7552.
47 O. P. Anderson, A. G. Barrett, J. J. Edmunds, S.-I. Hachiya, J. A. Hendrix, K. Horita, J. W. Malecha, C. J. Parkinson and A. VanSickle, *Can. J. Chem.*, 2001, **79**, 1562–1592.
48 J. Inanaga, K. Hirata, H. Saeki, T. Katsuki and M. Yamaguchi, *Bull. Chem. Soc. Jpn.*, 1979, **52**, 1989–1993.
49 A. K. Chatterjee and R. H. Grubbs, *Org. Lett.*, 1999, **1**, 1751–1753.
50 O. M. Ogba, N. C. Warner, D. J. O'Leary and R. H. Grubbs, *Chem. Soc. Rev.*, 2018, **47**, 4510–4544.
51 S. B. Garber, J. S. Kingsbury, B. L. Gray and A. H. Hoveyda, *J. Am. Chem. Soc.*, 2000, **122**, 8168–8179.
52 S. Gessler, S. Randl and S. Blechert, *Tetrahedron Lett.*, 2000, **41**, 9973–9976.
53 A. De Mico, R. Margarita, L. Parlanti, A. Vescovi and G. Piancatelli, *J. Org. Chem.*, 1997, **62**, 6974–6977.
54 A. E. J. d. Nooy, A. C. Besemer and H. v. Bekkum, *Synthesis*, 1996, 1153–1176.
55 D. B. Dess and J. C. Martin, *J. Org. Chem.*, 1983, **48**, 4155–4156.
56 S. Ho, D. L. Sackett and J. L. Leighton, *J. Am. Chem. Soc.*, 2015, **137**, 14047–14050.
57 J. D. Mortison, M. Schenone, J. A. Myers, Z. Zhang, L. Chen, C. Ciarlo, E. Comer, S. K. Natchiar, S. A. Carr, B. P. Klaholz and A. G. Myers, *Cell Chem. Biol.*, 2018, **25**, 1506–1518.
58 For recent work by our group on other complex bioactive macrolides, see: (*a*) A. W. Phillips, M. J. Anketell, T. Balan, N. Y. S. Lam, S. Williams and I. Paterson, *Org. Biomol. Chem.*, 2018, **16**, 8286–8291; (*b*) S. Williams, J. Jin, S. B. J. Kan, M. Li, L. J. Gibson and I. Paterson, *Angew. Chem., Int. Ed.*, 2017, **56**, 645–649; (*c*) N. Anžiček, S. Williams, M. P. Housden and I. Paterson, *Org. Biomol. Chem.*, 2018, **16**, 1343–1350; (*d*) N. Y. S. Lam, G. Muir, V. R. Challa, R. Britton and I. Paterson, *Chem. Commun.*, 2019, **55**, 9717–9720.